

Electric-field switching of interlayer magnetic order in a van der Waals heterobilayer via spin-electric potential

Received: 19 November 2024

Accepted: 14 October 2025

Published online: 24 November 2025

 Check for updatesChengxi Huang¹, Jinzhe Han¹, Jing Wang¹, Jintao Jiang¹, Ziyang Qu¹, Fang Wu², Ang Li¹, Yi Wan¹, Kaiyou Wang^{3,4}✉ & Erjun Kan¹✉

Electric-field control of magnetic order is of significant physical interest and holds great potential for spintronic applications. However, it has rarely been reported in two-dimensional (2D) van der Waals (vdW) magnets, primarily due to the inherently weak coupling between spin order and electric fields. Here we propose a general spin-electric potential mechanism that significantly enhances the magnetoelectric coupling. The spin-electric potential refers to the spin-order-dependent electric dipole potential energy originating from the polar spin interactions in asymmetric magnetic systems. Due to the additional spin-electric potential, the relative stability of different interlayer spin orders in a vdW heterobilayer can be significantly manipulated by external electric fields. Based on this mechanism, we design a series of 2D vdW all-magnetic heterobilayers, such as CrI₃/MnSe₂, in which a transition from interlayer spin-parallel (SP) to spin-antiparallel (SAP) order is realized by a feasible electric field of around 0.1 V/Å. Our findings not only reveal a novel magnetoelectric coupling mechanism, but also present a practical strategy for achieving pure electric field switching of magnetic order.

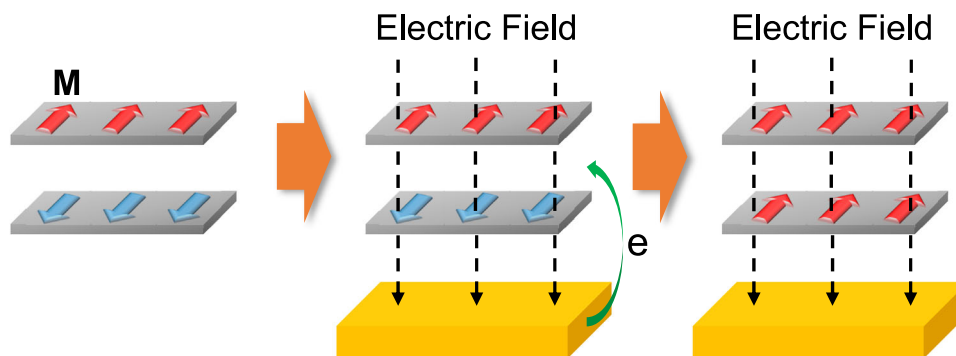
Modern magnetic memories primarily rely on a fundamental physical effect that the magnetoresistance of a magnetic tunnel junction (MTJ) can be significantly changed by switching its magnetic state. Controlling the magnetic state by an external electric field (voltage), rather than a current or magnetic field, has been a long-sought goal for developing next-generation, low-dissipation and high-efficiency spintronic devices, such as voltage-controlled magnetic random access memories^{1,2}. Interestingly, a giant tunneling magnetoresistance has also been observed in two-dimensional (2D) van der Waals (vdW) magnetic layers^{3–5}, since the discovery of 2D magnets^{6–12}. Such a magnetoresistance can be significantly modulated by altering the interlayer magnetic state through various external factors, such as magnetic fields¹³, mixed magnetic and electric fields^{14–17}, ferroelectric fields^{18,19}, strain²⁰, pressure^{21,22}, twisting^{23–25}, and spin injection²⁶. These

advancements have opened up a new avenue toward vdW spin-filter MJT²⁷. However, pure electric-field switching of interlayer magnetic order remains a significant challenge owing to the lack of an effective magnetoelectric coupling mechanism.

Generally, magnetoelectric coupling could be induced through spin-orbit, spin-lattice and/or spin-charge interactions²⁸. Although plenty of 2D vdW magnets have been discovered so far, electrical switching between interlayer spin-parallel (SP) and spin-antiparallel (SAP) orders has only been reported in the CrI₃ bilayer^{29–32}, driven by the charge transfer mechanism. As shown in Fig. 1a, extra electron or hole carriers transfer from the substrate to the vdW magnetic layers upon electrostatic gating, which increases the density of states at the Fermi level and typically leads to an SAP-to-SP order transition^{33,34}. However, the spin-charge interaction induced by interlayer charge

¹MIIT Key Laboratory of Semiconductor Microstructure and Quantum Sensing, Nanjing University of Science and Technology, Nanjing, P. R. China. ²College of Information Science and Technology, Nanjing Forestry University, Nanjing, Jiangsu, P. R. China. ³State Key Laboratory for Superlattices and Microstructures, Institute of Semiconductors, Chinese Academy of Sciences, Beijing, P. R. China. ⁴Center of Materials Science and Optoelectronics Engineering, University of Chinese Academy of Sciences, Beijing, China. ✉e-mail: kywang@semi.ac.cn; ekan@njjust.edu.cn

a Charge Transfer Mechanism



b Spin-electric Potential Mechanism

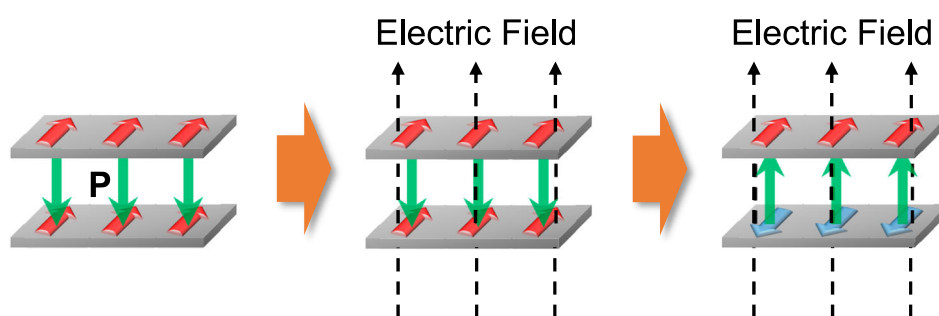


Fig. 1 | Interfacial magnetoelectric coupling mechanism. Schematic diagrams for electric-field switching of interlayer magnetic order driven by (a) charge transfer and (b) spin-electric potential mechanism. Gray and yellow slabs represent

magnetic vdW monolayers and non-magnetic substrates, respectively. Red and Blue arrows represent spin moments (M). Green arrows represent electric dipole moments (P).

transfer is commonly rather weak, so that the switching of interlayer magnetic order still requires the assistance of a strong external magnetic field. Therefore, a general mechanism to enhance the coupling between spin order and external electric field is urgently needed for achieving pure electric-field-driven interlayer magnetic order switching in 2D vdW magnets.

Here, we propose a general spin-electric-potential mechanism that in an asymmetric vdW magnetic bilayer, the interlayer polar spin interaction could lead to distinct different out-of-plane electric dipole moments for different interlayer spin orders. Consequently, under an external out-of-plane electric field, the SP and SAP orders gain very different electric dipole potential energies, which could reverse their relative stability (Fig. 1b). Based on a tight-binding dimer model, we reveal that the remarkable interplay between spin order and electric dipole moment originates from the disparity in occupation and spatial distribution of spin charges between SP and SAP states. Then, utilizing first-principles calculations, we predict a series of asymmetric vdW magnetic heterobilayers that exhibit strong magnetoelectric coupling driven by the spin-electric-potential mechanism. Especially, for the $\text{CrI}_3/\text{MnSe}_2$ heterobilayer, an SP-to-SAP phase transition could be realized by applying a feasible out-of-plane electric field around 0.1 V/\AA .

Results and discussion

The concept of spin-electric potential

It is known that an electric dipole can be reversed by external electric fields because of the electric dipole potential energy given by $W = -P \cdot \mathcal{E}$, where P is the electric dipole moment and \mathcal{E} is the electric field intensity (Fig. 2a). On the other hand, for a magnetic system, the

relative stability of the SP and SAP orders is determined by their energy difference, defined as $E_{\text{ex}} = E_{\text{SAP}} - E_{\text{SP}}$ (here E_{SP} and E_{SAP} are total energies of SP and SAP states, respectively). A positive (negative) value of E_{ex} indicates that the SP (SAP) states is the magnetic ground state. The E_{ex} can be a function of external magnetic fields owing to the magnetic potential energy, so that the SAP order could be switched to SP order by applying external magnetic fields (Fig. 2b). However, electric-field-switching of magnetic order is generally rather difficult because there is no direct interaction between a spin and an electric field.

Let's assume that there is an asymmetric magnetic dimer, which is inherently polar (Fig. 2c). The electric dipole potential energies for the SP and SAP states of the dimer are given by $W_{\text{SP}} = -P_{\text{SP}} \cdot \mathcal{E}$ and $W_{\text{SAP}} = -P_{\text{SAP}} \cdot \mathcal{E}$, respectively (here, P_{SP} and P_{SAP} are electric dipole moments for SP and SAP states, respectively). If $P_{\text{SAP}} \neq P_{\text{SP}}$, then there will be a difference between W_{SP} and W_{SAP} , which can be written as $\Delta W = W_{\text{SAP}} - W_{\text{SP}} = -(P_{\text{SAP}} - P_{\text{SP}}) \cdot \mathcal{E} = -P_{\text{ex}} \cdot \mathcal{E}$ (here $P_{\text{ex}} = P_{\text{SAP}} - P_{\text{SP}}$). Interestingly, owing to the presence of ΔW , the E_{ex} becomes a function of electric fields, namely, $E_{\text{ex}}(\mathcal{E}) = E_{\text{ex}}(\mathcal{E} = 0) + \Delta W = E_{\text{ex}}(\mathcal{E} = 0) - P_{\text{ex}} \cdot \mathcal{E}$, where $E_{\text{ex}}(\mathcal{E} = 0)$ represents the intrinsic E_{ex} under zero electric field. This equation can also be rewritten as $\Delta E_{\text{ex}}/\Delta \mathcal{E} = -P_{\text{ex}}$ [here, $\Delta E_{\text{ex}} = E_{\text{ex}}(\mathcal{E}') - E_{\text{ex}}(\mathcal{E})$ and $\Delta \mathcal{E} = \mathcal{E}' - \mathcal{E}$]. According to this equation, as long as the magnitude of P_{ex} is considerable, the relative stability of SP and SAP orders can be significantly manipulated by applying external electric fields. Here, we name such an additional spin-order-dependent electric dipole potential energy that modifies the relative stability of spin orders for an asymmetric magnetic system as spin-electric potential.

Now we consider an asymmetric vdW magnetic bilayer, which possesses out-of-plane electric polarizations and intralayer

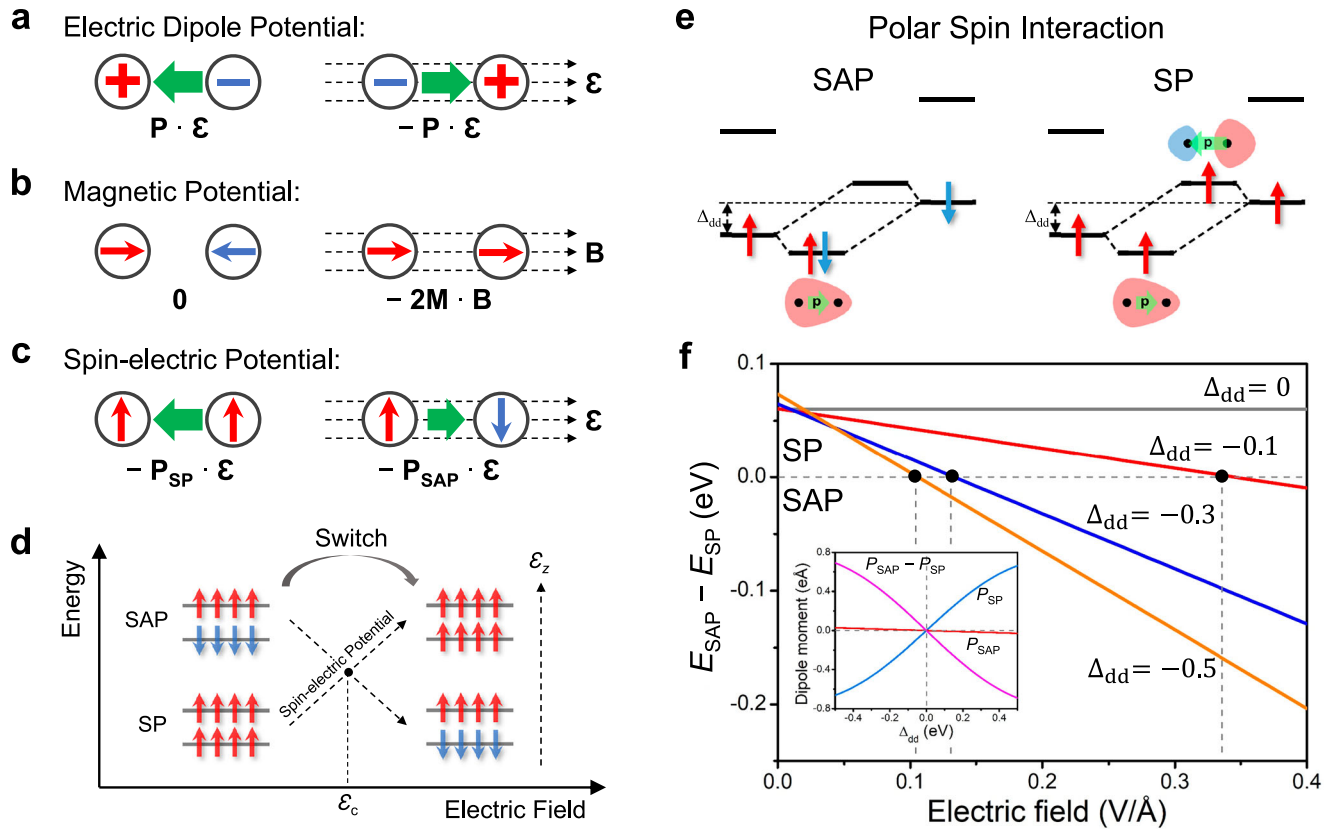


Fig. 2 | Spin-electric potential and driven magnetoelectric coupling mechanism. Schematic diagrams of (a) electric dipole potential, (b) magnetic potential, and (c) spin-electric potential. P , M , E and B represent electric dipole moment, magnetic moment, electric field intensity and magnetic field intensity, respectively. P_{SAP} and P_{SP} represent electric dipole moments of spin-antiparallel (SAP) and spin-parallel (SP) states, respectively. Red and blue arrows represent electron spins. Green arrows represent electric dipole moments. **d** Schematic diagram of electric-field switching of interlayer magnetic order driven by spin-electric potential. E_z represents the out-of-plane electric field, E_c represents the coercive electric field

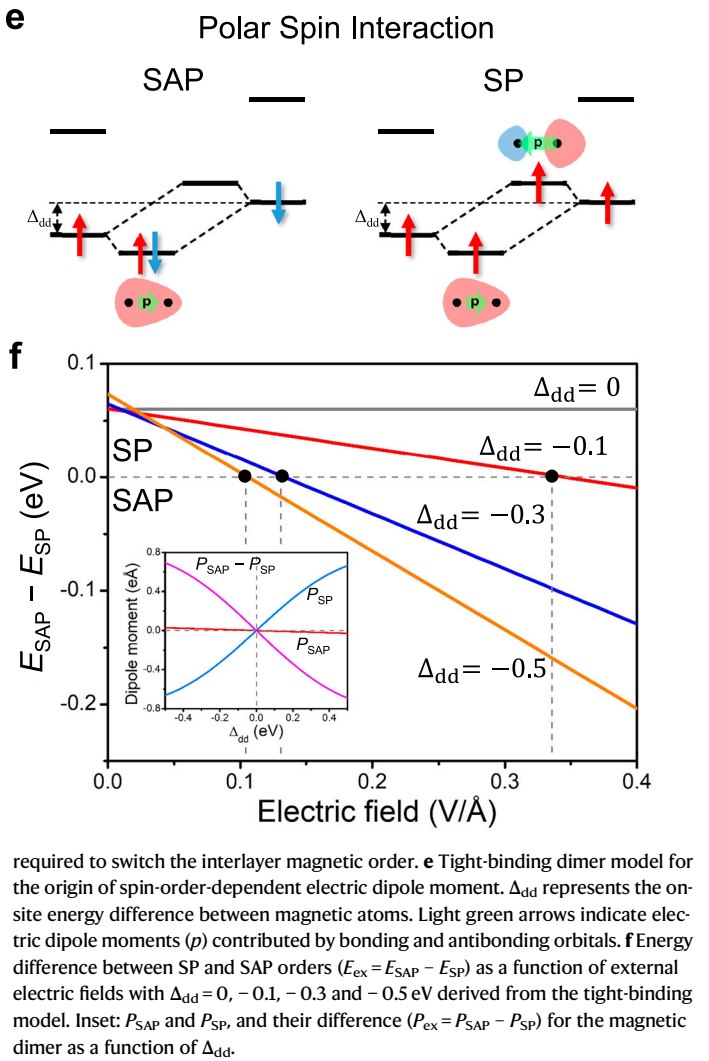
ferromagnetic orders in each layer. If the interlayer SP and SAP states have distinctly different out-of-plane electric dipole moments, namely $P_{SP} \neq P_{SAP}$. Then, owing to the spin-electric potential, the relative stability of the interlayer SP and SAP orders could be reversed by applying an out-of-plane electric field when the P_{ex} is large enough (Fig. 2d). However, the P_{ex} and corresponding magnetoelectric effects have never been reported in a vdW magnetic system. Whether and how an electric dipole moment interplays with the spin order is still unclear.

Tight-binding dimer model

To explore this, we firstly introduce a tight-binding dimer model³⁵ to explore the interplay between electric dipole moment and spin order. For simplicity, we adopted the one-dimensional Gaussian functions as the atomic basis functions to calculate the electron density and electric dipole moment (see supplementary section 1 for details). The general Hamiltonian of the dimer is written as

$$\hat{H} = \sum_{i,l,\sigma} \epsilon_{il} \hat{d}_{il\sigma}^\dagger \hat{d}_{il\sigma} + \sum_{i \neq j} \sum_{l,l',\sigma} (t_{il\sigma,jl'\sigma} \hat{d}_{il\sigma}^\dagger \hat{d}_{jl'\sigma} + h.c.) + \sum_{i,l} \frac{1}{2} U_i m_i \cdot S_{il} \quad (1)$$

where i and j are site (atom) index, l and l' are orbital index, and σ is spin index. The first, second and third terms represent the on-site energy of each orbital, the interatomic hopping and the spin-splitting under the mean field approximation, respectively.



In the magnetic dimer, each atom has two orbitals and one localized spin (Fig. 2e). If we introduce an on-site orbital energy difference (Δ_{dd}) between the two magnetic atoms, the polar spin interaction will induce an electric dipole moment, which is totally contributed by the spatial disproportion of spin charges and, thus, could be sensitive to the spin order. In the SAP order, the occupied eigenstates are both bonding states (Supplementary Fig. 1d). Whereas in the SP order, the lowest eigenstate is a bonding state while the second-lowest eigenstate is an antibonding state (Supplementary Fig. 1e). This disparity in occupation states leads to a significant redistribution of spin charges and, thus, induces a distinct P_{ex} . The magnitude of P_{ex} is positively correlated with the magnitude of Δ_{dd} (inset in Fig. 2f). Consequently, the E_{ex} is more sensitive to the electric field when the Δ_{dd} is larger (Fig. 2f) according to the equation $\Delta E_{ex}/\Delta E = -P_{ex}$. Furthermore, if we ignore the electric field effects on the Δ_{dd} and P_{ex} , then we obtain $E_c = E_{ex}(\mathcal{E}=0)/P_{ex}$, where E_c is defined as the critical electric field that makes the E_{ex} become zero, namely $E_{ex}(\mathcal{E}=E_c) = 0$. Supplementary Fig. 5b shows that the $E_{ex}(\mathcal{E}=0)$ is only slightly affected by Δ_{dd} . Therefore, the magnitude of E_c could be reduced by increasing the magnitude of Δ_{dd} (Fig. 2f and Supplementary Fig. 5c). On the other hand, the P_{ex} , $E_{ex}(\mathcal{E}=0)$, and E_c are also affected by the interatomic hopping integral (t) (Supplementary Fig. 2c and Fig. 5). Overall, the model analysis results indicate that the P_{ex} and spin-electric potential originate from the polar spin interactions in an asymmetric magnetic system with nonzero Δ_{dd} .

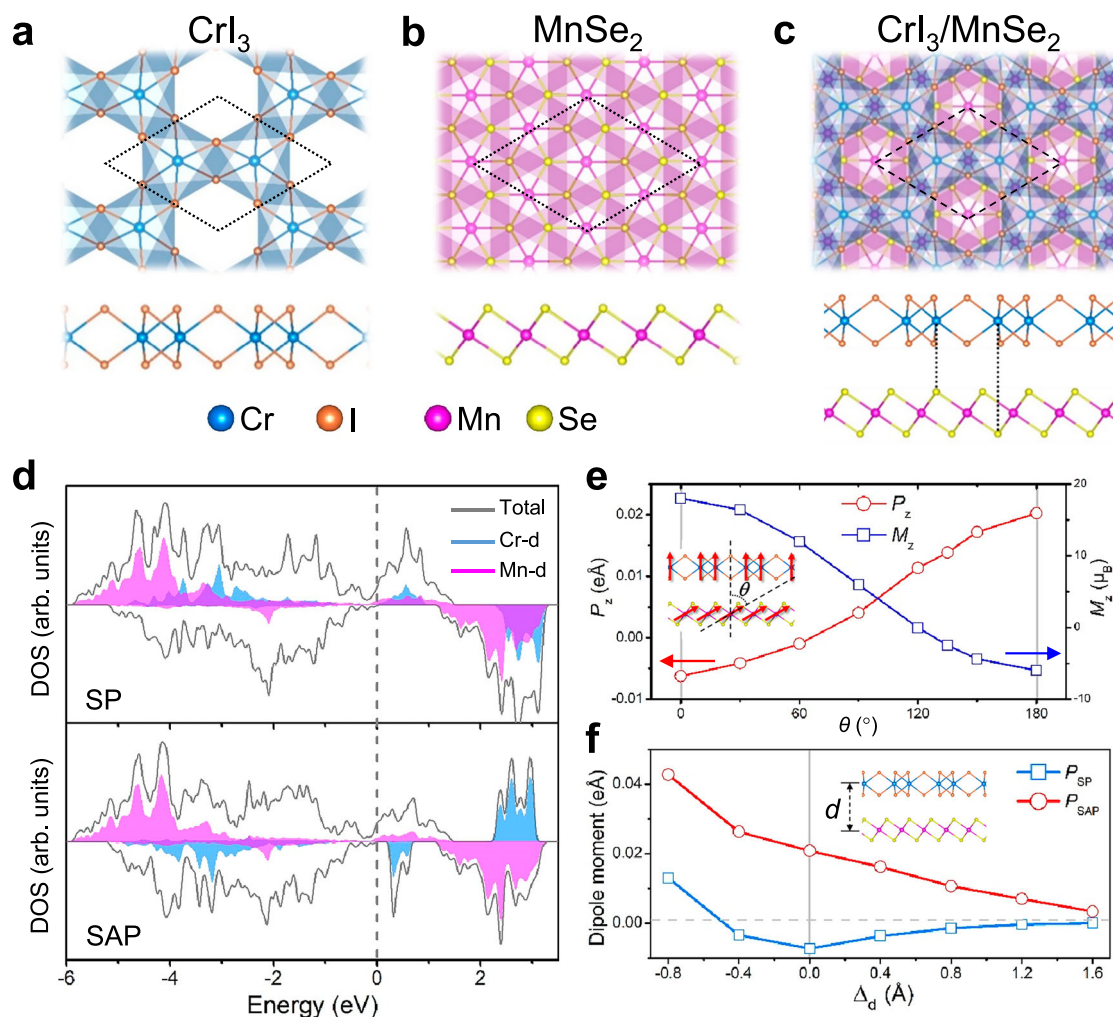


Fig. 3 | CrI₃/MnSe₂ vdW heterobilayer. Top (upper panels) and side (lower panels) views of the optimized atomic structures for (a) CrI₃, (b) MnSe₂ monolayers and (c) CrI₃/MnSe₂ heterobilayer. Blue, orange, purple and yellow balls represent Cr, I, Mn and Se ions, respectively. **d** Projected density of states for the SP and SAP states of the CrI₃/MnSe₂ heterobilayer. The gray dashed line represents the Fermi level.

e Out-of-plane electric dipole moment (P_z) and z-component of magnetic moment (M_z) per unit cell as a function of the angle (θ) between the spins in the two magnetic layers. **f** The P_{SP} and P_{SAP} as a function of the change of interlayer distance (d) with respect to the equilibrium state.

Magnetic heterodimer

One alternative way to introduce an intrinsic large Δ_{dd} in a realistic magnetic system is choosing different transition metal atoms to construct a magnetic heterostructure. The simplest magnetic heterostructure is the transition metal heterodimer, e.g., MnCr dimer. Our first-principles calculation results (Supplementary Fig. 6) show that, for the MnCr dimer, the P_{SAP} is indeed distinctly different from the P_{SP} , resulting in a large P_{ex} (> 0.06 eÅ) when the interatomic distance (r) is ranging from 3.2 to 4.2 Å. Such a large P_{ex} is mainly contributed by the direct polar spin interactions between Mn- and Cr- d_{z^2} orbitals with a Δ_{dd} of ~ 5.1 eV (see supplementary section 2 for more details). These calculation results are consistent with the tight-binding model analysis results.

vdW magnetic heterobilayer

A vdW all-magnetic heterostructure, in which each layer has a different magnetic transition metal atom, may also possess a sizable Δ_{dd} . Therefore, here we focus on a vdW all-magnetic heterobilayer, i.e., CrI₃/MnSe₂, to explore the interplay between out-of-plane electric dipole moment and interlayer spin order. The CrI₃ (Fig. 3a) and MnSe₂ (Fig. 3b) monolayers have both been predicted and experimentally confirmed to be 2D ferromagnetic materials^{7,10}. Individually, they are

both centrosymmetric and non-polar. Since the lateral lattice constants of CrI₃ (6.98 Å) are much larger than that of MnSe₂ (3.61 Å), we used a 2×2 supercell of MnSe₂ to construct the CrI₃/MnSe₂ heterobilayer (with a lattice mismatch of $\sim 3.4\%$). Figure 3c shows the optimal stacking structure for both interlayer SP and SAP orders (see supplementary section 3 for details), which has in-plane c_3 symmetry and, thus, an out-of-plane electric polarization. Notably, the P_{SAP} and P_{SP} are calculated to be 0.0202 and -0.0073 eÅ/u.c., respectively, with a positive value indicates the direction pointing from MnSe₂ to CrI₃. The P_{ex} is 0.0275 eÅ/u.c. Note that, although the system is metallic in the periodic (in-plane) direction, electric polarization along the non-periodic (out-of-plane) direction is well-defined and is tunable by applying out-of-plane electric fields, as demonstrated in the metallic WTe₂ multilayers³⁶.

To understand the origin of such a large P_{ex} for CrI₃/MnSe₂, we firstly compare the atomic structures of SAP and SP states and find that the structural difference is quite small (see supplementary section 3 for details). Even though we use the same atomic structure for SAP and SP states without structural optimization, the obtained P_{SAP} , P_{SP} and P_{ex} are 0.0216, -0.0056 and 0.0272 eÅ/u.c., respectively, very close to those of the optimized CrI₃/MnSe₂. Therefore, the small structural distortion (ionic polarization) is not the main origin of the large P_{ex} .

Next, we investigate the electronic polarization driven by the interlayer polar spin interactions (see supplementary section 3 for details). Different from the MnCr dimer, the ligands on the inner surfaces of the CrI₃/MnSe₂ also play an important role. The charge accumulation in the interlayer space (Supplementary Fig. 10) implies an interlayer covalent interaction, which is dominated by Se- and I-pz orbitals (Supplementary Figs. 11 and 14). This provides a sizable indirect d-p-d super-exchange interaction between Cr and Mn ions. On the other hand, Fig. 3d shows a distinct energy difference between Cr-3d and Mn-3d orbitals, implying a large Δ_{dd} , which is estimated to be ~1.41 eV (Supplementary Fig. 14c). Therefore, the P_{ex} of the CrI₃/MnSe₂ can also be qualitatively explained by the aforementioned dimer model. Nevertheless, the P_{ex} of the CrI₃/MnSe₂ is distinctly smaller than that of the MnCr dimer. This is because the indirect interlayer spin interactions in the CrI₃/MnSe₂ are generally weaker than the direct interactions in the MnCr dimer.

The spin-order-dependent electric dipole moments have also been observed in other vdW magnetic heterobilayers (see supplementary section 4 for details). These results indicate that the magnitude of P_{ex} can be manipulated by changing the types of transition metal and/or ligand ions. For instance, the CrI₃/MnSe₂ exhibits a much larger $|P_{ex}|$ (0.0275 eÅ/u.c.) than the CrI₃/CrSe₂ (0.0015 eÅ/u.c.) does. This is because the Δ_{dd} between the same TM atoms (e.g., Cr) in different layers is generally much smaller than that between different TM atoms (e.g., Cr and Mn). Besides, the CrI₃/MnX₂ (X = S, Se, Te) systems show an increasing magnitude of P_{ex} (0.0040, 0.0275 and 0.0713 eÅ/u.c.) from S to Se, and to Te. This can be understood as the fact that (i) the 3p, 4p and 5p orbitals for the S, Se and Te atoms are more and more delocalized as the atomic size increasing. A more delocalized orbital usually manifests a larger spatial charge disproportion, thereby, leads to a larger electric polarization. (ii) As the electronegativity decreases from S to Se, and to Te, the metal-chalcogen covalent interactions become stronger (Supplementary Fig. 17), which enhances the interlayer super-exchange interactions and enlarges the P_{ex} . Similar behavior also occurs in the CrGeTe₃/MnX₂ (X = S, Se, Te) systems.

To directly show the magnetoelectric effect in CrI₃/MnSe₂, we considered a possible spin-order-transition process characterized by the collective rotation of spins in each layer. By gradually changing the angle (θ) between the spins in the two magnetic layers from 0 to 180° ($\theta = 0$ and 180° corresponding to SP and SAP states, respectively), we obtain a continuous change of out-of-plane electric dipole moment (from -0.0073 to 0.0202 eÅ/u.c.) and total magnetic moment along z-axis (from 18 to -6 μ_B /u.c.) with respect to the θ (Fig. 3e), which indicates a strong interfacial magnetoelectric coupling. Besides, from the relative energy profiles (Supplementary Fig. 18), we find a rather small activation barrier (< 0.5 meV/u.c.) for the spin-order-transition, suggesting that the transition from a high-energy to the ground-state spin order could occur under ambient conditions.

The relation between interlayer distance and magnetoelectric property of the CrI₃/MnSe₂ has also been investigated. Supplementary Fig. 15 shows a Bethe-Slater-curve-like relation between E_{ex} and interlayer distance, which has also been observed in other magnetic bilayers (e.g., CrSe₂)³⁷. Figure 3f shows that the P_{SAP} monotonously increases, while the P_{SP} first decreases and then increases as the interlayer distance decreasing. These profiles can also be reproduced by our dimer model by combining the contribution of non-magnetic and magnetic atoms to the electric dipole moments (Supplementary Fig. 2e).

Electric field effect on magnetic order

Now we explore the response of E_{ex} to external out-of-plane electric fields and its relation with P_{ex} for vdW magnetic bilayers. As shown in Fig. 4a and Supplementary Fig. 19, the $\Delta E_{ex}/\Delta \mathcal{E}_z$ (\mathcal{E}_z is the out-of-plane electric field intensity), namely the slope of the profiles, is distinctly different for different magnetic bilayers and is closely related with the P_{ex} . For instance, when the \mathcal{E}_z increases from 0 to 0.2 V/Å (positive

values of \mathcal{E}_z indicate the direction pointing from MnSe₂ to CrI₃), the $|\Delta E_{ex}|$ of CrI₃ bilayer is only 0.14 meV, while that of CrI₃/MnSe₂ is as large as 6.91 meV. Correspondingly, the P_{ex} of CrI₃ bilayer and CrI₃/MnSe₂ are zero and 0.0275 eÅ/u.c., respectively. Therefore, a sizable P_{ex} can significantly increase the magnitude of $\Delta E_{ex}/\Delta \mathcal{E}_z$. Besides, for a symmetric magnetic bilayer (e.g., CrI₃ bilayer) with zero P_{ex} , the $E_{ex}(\mathcal{E}_z)$ and $E_{ex}(-\mathcal{E}_z)$ are equal (see the inset in Fig. 4a). While for an asymmetric magnetic heterobilayer with a sizable P_{ex} , the E_{ex} is basically a monotonic function of \mathcal{E}_z . More interestingly, by fitting the calculation results of a series of vdW magnetic heterobilayers, we obtained a nearly linear relationship between the $\Delta E_{ex}/\Delta \mathcal{E}_z$ and the P_{ex} (Fig. 4b), namely $\Delta E_{ex}/\Delta \mathcal{E}_z \approx -P_{ex}$, which demonstrates our aforementioned hypothesis. These indicate that the spin-electric potential mechanism is generally applicable and has a dominant effect on the magneto-electric response for an asymmetric vdW magnetic system with a sizable P_{ex} (see supplementary section 5 for details).

The $E_{ex}(\mathcal{E}_z = 0)$ is also an important parameter for realizing electric-field-driven magnetic order switching. Supplementary Table 3 shows that the magnitude of $E_{ex}(\mathcal{E}_z = 0)$ for a vdW magnet is usually ranging from several to dozens of meV/u.c. Such a large $E_{ex}(\mathcal{E}_z = 0)$ could make the electric-field, even the magnetic-field control of interlayer magnetic order very difficult. However, according to the equation $\mathcal{E}_c = E_{ex}(\mathcal{E}_z = 0)/P_{ex}$ derived from the spin-electric-potential mechanism, as long as the P_{ex} reaches several 0.01 eÅ/u.c., the \mathcal{E}_c could be reduced to the order of magnitude of 0.1 V/Å, which is feasible in experiments. Besides, we find that the $E_{ex}(\mathcal{E}_z = 0)$ is usually sensitive to interlayer stacking^{22,38-40} (Supplementary Fig. 9b) and in-plane strain^{20,41} (Supplementary Fig. 20), while the P_{ex} is not. For instance, for the CrI₃/MnSe₂, the $E_{ex}(\mathcal{E}_z = 0)$ greatly changes from 13.10 to -35.85 meV/u.c., while the P_{ex} slightly changes from 0.0201 to 0.0298 eÅ/u.c., when the in-plane strain increases from -4% to 4%. Therefore, the \mathcal{E}_c can also be manipulated by controlling the interlayer stacking or applying an external in-plane strain.

Owing to the large P_{ex} of 0.0275 eÅ/u.c., the E_{ex} of the CrI₃/MnSe₂ is very sensitive to the \mathcal{E}_z (Fig. 4c). A \mathcal{E}_z greater than -0.1 V/Å will change its E_{ex} from 2.66 meV/u.c. to a negative value and, thus, switch the interlayer spin order from SP to SAP (Supplementary Fig. 18b). The relation between these values is consistent with the equation $\mathcal{E}_c = E_{ex}(\mathcal{E}_z = 0)/P_{ex} = 0.00266 \text{ eV}/0.0275 \text{ eÅ} \approx 0.1 \text{ V/Å}$. This mechanism can cause not only an SP-to-SAP, but also an SAP-to-SP phase transition. For instance, a tensile in-plane strain of 1% changes the interlayer spin order of CrI₃/MnSe₂ to SAP with $E_{ex}(\mathcal{E}_z = 0) = -4.46 \text{ meV/u.c.}$ while the P_{ex} barely changes. Then, a negative \mathcal{E}_z greater than 0.16 V/Å in magnitude could switch the interlayer spin order from SAP to SP (Fig. 4c).

It is worth noting that the charge transfer mechanism cannot explain the electric-field switching of interlayer magnetic order in the CrI₃/MnSe₂. Generally, charge transfer (electrostatic doping) benefits the SAP-to-SP phase transition. In the CrI₃/MnSe₂, the inherent interlayer charge transfer for the SAP state is -0.018 e/u.c., with negative values indicate a net electron transfer from CrI₃ to MnSe₂ layer (Fig. 4d). In this case, applying a negative out-of-plane electric field (pointing from CrI₃ to MnSe₂ layer) suppresses the interlayer charge transfer, however, benefits the SP phase. This violates the charge transfer mechanism. Therefore, our proposed spin-electric-potential mechanism provides a new angle of view to understand the electric-field switching of magnetic order.

In summary, utilizing a tight-binding dimer model and first-principles calculations, we have proposed a general mechanism of realizing electric-field switching of interlayer magnetic order in a vdW magnetic system by introducing the concept of spin-electric potential. The spin-electric potential is an additional spin-order-dependent electric dipole potential energy that modifies the relative stability of spin orders. It originates from the polar spin interaction (with $\Delta_{dd} \neq 0$) in an asymmetric magnetic structure. The polar spin interaction causes a distinct difference on occupation and spatial distribution of spin

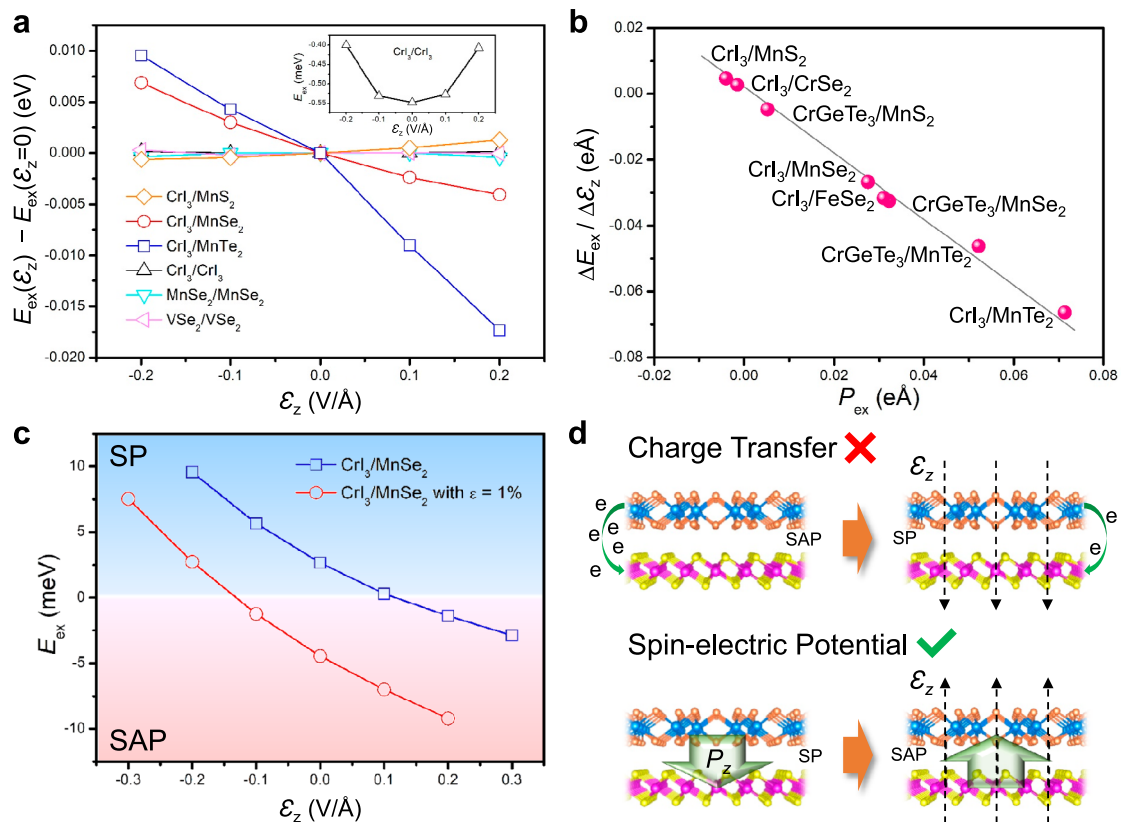


Fig. 4 | Electric field effects on interlayer magnetic coupling. **a** The change of E_{ex} as a function of E_z for different vdW magnetic bilayers. A positive value of E_z indicates the out-of-plane direction pointing from MnX_2 ($X = \text{S}, \text{Se}, \text{Te}$) to CrI_3 layer. **b** The nearly linear relation between $\Delta E_{\text{ex}}/\Delta E_z$ and P_{ex} . Without loss of generality,

here we take $\Delta E_{\text{ex}}/\Delta E_z = [E_{\text{ex}}(E_z = 0.1) - E_{\text{ex}}(E_z = -0.1)]/0.2$. The gray line indicates the linear fitting of the calculation results. **c** E_{ex} as a function of E_z for $\text{CrI}_3/\text{MnSe}_2$ bilayer without and with an in-plane biaxial tensile strain of 1%. **d** Comparison between charge transfer and spin-electric-potential mechanism in the $\text{CrI}_3/\text{MnSe}_2$.

charges between SAP and SP states, leading to a sizable P_{ex} . The nearly linear relation between the $\Delta E_{\text{ex}}/\Delta E_z$ and the P_{ex} , namely, $\Delta E_{\text{ex}}/\Delta E_z = -P_{\text{ex}}$, demonstrates that the magnetoelectric effect is dominated by the spin-electric-potential mechanism. Consequently, by inducing a sizable P_{ex} via constructing a vdW all-magnetic heterostructure, a pure electric-field switching of interlayer magnetic order could be achieved, as predicted in the $\text{CrI}_3/\text{MnSe}_2$ and other vdW magnetic heterobilayers. These findings will be of great interest for developing pure voltage-controlled vdW spin-filter MTJs. We look forward to experimental observation in the future.

Methods

Computational methods

The first-principles calculations based on density functional theory were carried out using the Vienna Ab initio Simulation Package⁴². The PBE + U calculations⁴³ with $U_{\text{eff}} = 3$ eV for 3d electrons of transition metal atoms (e.g., Cr and Mn) according to the Dudarev's method⁴⁴ was employed to treat the exchange-correlation and strong electronic correlation. We have also repeated our calculations on the $\text{CrI}_3/\text{MnSe}_2$ using different calculation methods, i.e., the PBE + U method with U_{eff} values ranging from 2 to 4 eV for Cr- and Mn-3d orbitals, the meta-GGA SCAN and the hybrid HSE06 functionals. The results show that the choice of different calculation methods barely affects the main conclusion (Supplementary Table 2). The energy cutoff for the plane wave⁴⁵ was 500 eV. A Γ -centered $12 \times 12 \times 1$ Monkhorst-Pack⁴⁶ grid was used to sample the Brillouin zone. The vdW correction⁴⁷ was included. To avoid the incorrect periodic interactions along the c axis, a vacuum slab of ~ 30 Å and the dipole-dipole interaction corrections⁴⁸ were adopted. The energy and force convergence criteria were 1×10^{-6} eV and 0.005 eV/Å, respectively. The out-of-plane electric dipole moment

was calculated by integrating the electron density times the coordination over the whole unit cell.

Data availability

The data that support the findings of this study are provided in the supplementary information. Source data are provided in this paper.

References

- Fert, A., Ramesh, R., Garcia, V., Casanova, F. & Bibes, M. Electrical control of magnetism by electric field and current-induced torques. *Rev. Mod. Phys.* **96**, 015005 (2024).
- Matsukura, F., Tokura, Y. & Ohno, H. Control of magnetism by electric fields. *Nat. Nanotechnol.* **10**, 209–220 (2015).
- Song, T. et al. Giant tunneling magnetoresistance in spin-filter van der Waals heterostructures. *Science* **360**, 1214–1218 (2018).
- Zhu, W. et al. Large tunneling magnetoresistance in van der Waals ferromagnet/semiconductor heterojunctions. *Adv. Mater.* **33**, 2104658 (2021).
- Zhu, W. et al. Large room-temperature magnetoresistance in van der Waals ferromagnet/semiconductor junctions. *Chin. Phys. Lett.* **39**, 128501 (2022).
- Gong, C. et al. Discovery of intrinsic ferromagnetism in two-dimensional van der Waals crystals. *Nature* **546**, 265–269 (2017).
- Huang, B. et al. Layer-dependent ferromagnetism in a van der Waals crystal down to the monolayer limit. *Nature* **546**, 270–273 (2017).
- Deng, Y. et al. Gate-tunable room-temperature ferromagnetism in two-dimensional Fe_3GeTe_2 . *Nature* **563**, 94–99 (2018).
- Bonilla, M. et al. Strong room-temperature ferromagnetism in VSe_2 monolayers on van der Waals substrates. *Nat. Nanotechnol.* **13**, 289–293 (2018).

10. O'Hara, D. J. et al. Room temperature intrinsic ferromagnetism in epitaxial manganese selenide films in the monolayer limit. *Nano Lett.* **18**, 3125–3131 (2018).
11. Lee, K. et al. Magnetic order and symmetry in the 2D semiconductor CrSBr. *Nano Lett.* **21**, 3511–3517 (2021).
12. Zhang, X. et al. Room-temperature intrinsic ferromagnetism in epitaxial CrTe₂ ultrathin films. *Nat. Commun.* **12**, 2492 (2021).
13. Zhu, W. et al. Large and tunable magnetoresistance in van der Waals ferromagnet/semiconductor junctions. *Nat. Commun.* **14**, 5371 (2023).
14. Wang, Z. et al. Electric-field control of magnetism in a few-layered van der Waals ferromagnetic semiconductor. *Nat. Nanotechnol.* **13**, 554–559 (2018).
15. Liang, S. et al. Small-voltage multiferroic control of two-dimensional magnetic insulators. *Nat. Electron.* **6**, 199–205 (2023).
16. Wang, Z.-A. et al. Selectively controlled ferromagnets by electric fields in van der Waals ferromagnetic heterojunctions. *Nano Lett.* **23**, 710–717 (2023).
17. Xu, R. & Zou, X. Electric field-modulated magnetic phase transition in van der Waals CrI₃ bilayers. *J. Phys. Chem. Lett.* **11**, 3152–3158 (2020).
18. Cheng, H.-X., Zhou, J., Wang, C., Ji, W. & Zhang, Y. Ni. Nonvolatile electric field control of magnetism in bilayer CrI₃ on monolayer In₂Se₃. *Phys. Rev. B* **104**, 064443 (2021).
19. Li, P., Zhou, X.-S. & Guo, Z.-X. Intriguing magnetoelectric effect in two-dimensional ferromagnetic/perovskite oxide ferroelectric heterostructure. *NPJ Comput. Mater.* **8**, 20 (2022).
20. Cenker, J. et al. Reversible strain-induced magnetic phase transition in a van der Waals magnet. *Nat. Nanotechnol.* **17**, 256–261 (2022).
21. Li, T. et al. Pressure-controlled interlayer magnetism in atomically thin CrI₃. *Nat. Mater.* **18**, 1303–1308 (2019).
22. Song, T. et al. Switching 2D magnetic states via pressure tuning of layer stacking. *Nat. Mater.* **18**, 1298–1302 (2019).
23. Chen, Y. et al. Twist-assisted all-antiferromagnetic tunnel junction in the atomic limit. *Nature* **632**, 1045–1051 (2024).
24. Xie, H. et al. Twist engineering of the two-dimensional magnetism in double bilayer chromium triiodide homostructures. *Nat. Phys.* **18**, 30–36 (2022).
25. Xu, Y. et al. Coexisting ferromagnetic–antiferromagnetic state in twisted bilayer CrI₃. *Nat. Nanotechnol.* **17**, 143–147 (2022).
26. Min, K. H. et al. Tunable spin injection and detection across a van der Waals interface. *Nat. Mater.* **21**, 1144–1149 (2022).
27. Yang, H. et al. Two-dimensional materials prospects for non-volatile spintronic memories. *Nature* **606**, 663–673 (2022).
28. Dong, S., Xiang, H. & Dagotto, E. Magnetoelectricity in multiferroics: a theoretical perspective. *Nat. Sci. Rev.* **6**, 629–641 (2019).
29. Jiang, S., Shan, J. & Mak, K. F. Electric-field switching of two-dimensional van der Waals magnets. *Nat. Mater.* **17**, 406–410 (2018).
30. Huang, B. et al. Electrical control of 2D magnetism in bilayer CrI₃. *Nat. Nanotechnol.* **13**, 544–548 (2018).
31. Jiang, S., Li, L., Wang, Z., Mak, K. F. & Shan, J. Controlling magnetism in 2D CrI₃ by electrostatic doping. *Nat. Nanotechnol.* **13**, 549–553 (2018).
32. Song, T. et al. Voltage control of a van der Waals spin-filter magnetic tunnel junction. *Nano Lett.* **19**, 915–920 (2019).
33. Lu, Y., Wang, H., Wang, L. & Yang, L. Mechanism of carrier doping induced magnetic phase transitions in two-dimensional materials. *Phys. Rev. B* **106**, 205403 (2022).
34. Ghosh, S., Stojić, N. & Binggeli, N. Overcoming the asymmetry of the electron and hole doping for magnetic transitions in bilayer CrI₃. *Nanoscale* **13**, 9391–9401 (2021).
35. Huang, C. et al. Toward intrinsic room-temperature ferromagnetism in two-dimensional semiconductors. *J. Am. Chem. Soc.* **140**, 11519 (2018).
36. Fei, Z. et al. Ferroelectric switching of a two-dimensional metal. *Nature* **560**, 336–339 (2018).
37. Wang, C. et al. Bethe-Slater-curve-like behavior and interlayer spin-exchange coupling mechanisms in two-dimensional magnetic bilayers. *Phys. Rev. B* **102**, 020402 (2020).
38. Sivadas, N., Okamoto, S., Xu, X., Fennie, C. J. & Xiao, D. Stacking-dependent magnetism in bilayer CrI₃. *Nano Lett.* **18**, 7658–7664 (2018).
39. Jiang, P. et al. Stacking tunable interlayer magnetism in bilayer. *Phys. Rev. B* **99**, 144401 (2019).
40. Yang, S. et al. Controlling the 2D magnetism of CrBr₃ by van der Waals stacking engineering. *J. Am. Chem. Soc.* **145**, 28184–28190 (2023).
41. Liu, N. et al. Intralayer strain tuned interlayer magnetism in bilayer CrSBr. *Phys. Rev. B* **109**, 214422 (2024).
42. Kresse, G. & Hafner, J. Ab initio molecular dynamics for liquid metals. *Phys. Rev. B* **47**, 558 (1993).
43. Perdew, J. P., Burke, K. & Ernzerhof, M. Generalized gradient approximation made simple. *Phys. Rev. Lett.* **77**, 3865 (1996).
44. Dudarev, S. L., Botton, G. A., Savrasov, S. Y., Humphreys, C. J. & Sutton, A. P. Electron-energy-loss spectra and the structural stability of nickel oxide: An LSDA+U study. *Phys. Rev. B* **57**, 1505 (1998).
45. Blöchl, P. E. Projector augmented-wave method. *Phys. Rev. B* **50**, 17953 (1994).
46. Monkhorst, H. J. & Pack, J. D. Special points for Brillouin-zone integrations. *Phys. Rev. B* **13**, 5188 (1976).
47. Grimme, S. Semiempirical GGA-type density functional constructed with a long-range dispersion correction. *Comput. Chem.* **27**, 1787 (2006).
48. Makov, G. & Payne, M. C. Periodic boundary conditions in ab initio calculations. *Phys. Rev. B* **51**, 4014 (1995).

Acknowledgements

This work was supported by the Ministry of Science and Technology of the People's Republic of China (Nos. 2022YFA1402901, 2022YFA1405100), by the National Natural Science Foundation of China (Nos. T2125004, 12274227, U24A2010, 12241405, 12004183), and by the Fundamental Research Funds for the Central Universities (No. 30921011214, No. 30920041115). C.H. and E.K. acknowledge the support from the Tianjing Supercomputer Center and Shanghai Supercomputer Center.

Author contributions

E.K., C.H., and K.W. conceived the idea and supervised the project. C.H. performed calculations and data analysis. E.K., C.H., and K.W. drafted the manuscript. J.H., J.W., J.J., Z.Q., F.W., A.L., and Y.W. discussed the results and commented on the manuscript at all stages.

Competing interests

The authors declare no competing interests.

Additional information

Supplementary information The online version contains supplementary material available at <https://doi.org/10.1038/s41467-025-65371-1>.

Correspondence and requests for materials should be addressed to Kaiyou Wang or Erjun Kan.

Peer review information *Nature Communications* thanks Geunseok Lee, Zhenxiang Cheng and the other anonymous reviewer(s) for their contribution to the peer review of this work. A peer review file is available.

Reprints and permissions information is available at <http://www.nature.com/reprints>

Publisher's note Springer Nature remains neutral with regard to jurisdictional claims in published maps and institutional affiliations.

Open Access This article is licensed under a Creative Commons Attribution-NonCommercial-NoDerivatives 4.0 International License, which permits any non-commercial use, sharing, distribution and reproduction in any medium or format, as long as you give appropriate credit to the original author(s) and the source, provide a link to the Creative Commons licence, and indicate if you modified the licensed material. You do not have permission under this licence to share adapted material derived from this article or parts of it. The images or other third party material in this article are included in the article's Creative Commons licence, unless indicated otherwise in a credit line to the material. If material is not included in the article's Creative Commons licence and your intended use is not permitted by statutory regulation or exceeds the permitted use, you will need to obtain permission directly from the copyright holder. To view a copy of this licence, visit <http://creativecommons.org/licenses/by-nc-nd/4.0/>.

© The Author(s) 2025